OTC 11997

Norwegian Deepwater Program: Analysis of Vortex-Induced Vibrations of Marine Risers Based on Full-Scale Measurements

Karl E. Kaasen, Norwegian Marine Technology Research Institute (MARINTEK), Halvor Lie, MARINTEK (USA) Inc., Frøydis Solaas, MARINTEK, and J. Kim Vandiver, Massachusetts Institute of Technology

This paper was prepared for presentation at the 2000 Offshore Technology Conference held in Houston, Texas, 1–4 May 2000.

Abstract

As a part of the Norwegian Deepwater Program (NDP) three drilling risers have been instrumented with accelerometers and rotation-rate meters for measurement of vortex-induced vibrations (VIV). In addition, current was measured at number of depths. The paper describes how the riser displacements were derived from the measurements and compared with the current. A major task has been to rid the acceleration measurements of the influence of gravity due to the riser's rotations out of the vertical and include the measurements of angular motion in a consistent way. This has been done using modal decomposition and a least-squares method to estimate the modal weights. The main purpose of the work was to provide data for calibration of computer programs for prediction of VIV. Examples of results are given.

Introduction

To design marine risers for use in deep waters it is important to be able to predict the character and amount of vortex-induced vibration the riser may have. In general VIV will be important with respect to fatigue as well as drag forces on the riser.

The VIV response of a marine riser is a complicated pro??cess involving both the hydrodynamical and the structural properties of the riser. Model testing has given valuable insight in VIV. Different types of experimenting have been done, e.g. forced motion with rigid cylinders in a uniform flow (Ref. 1), spring-supported rigid cylinders in uniform flow (Ref 2) and scaled riser models in uniform and sheared flows (Ref. 3). Ref. 4 gives a comprehensive introduction to the phenomenon of VIV in general, while Ref. 5 is an account of the state of art when it comes to VIV of marine risers.

Still, full-scale data are needed to verify VIV models at realistic Reynolds numbers and in realistic currents that vary with depth. The task of obtaining data by instrumentation and processing of the measurements is not trivial and, if done incorrectly, may lead to results of questionable value.

In order to provide full-scale data for VIV verification, three drilling risers at fields offshore North Norway had been instrumented for measurement of riser response. Also the sea current was measured at a number of depths. The three fields were Nyk High, Vema and Helland-Hansen. The water depths at these sites are 1270 m (Nyk High), 1220 m (Vema) and 685 m (Helland-Hansen). The instrumentation at these sites differed mainly in details, e.g. the number of motion and current sensors.

To use full-scale measurements in verification it is very important that the measurements are processed correctly before use. Such processing will in general be necessary in order to convert the data to a form that is suitable for the verification. The typical device for measurement of riser dynamics is the accelerometer. Apart from general filtering to remove unwanted noise and bias, it is very important that the signal from the accelerometer is corrected for the time-varying disturbance by the gravitational acceleration. Neglecting this and integrating the accelerometer outputs twice to obtain (hopefully) displacement may lead to significant error.

The paper describes the method for processing and analysis that were applied to a large number of records of riser motion and current. The purpose of the analysis was to derive quantities that give meaningful information about the VIV phenomenon and could be used further for calibration of VIV-prediction tools such as SHEAR7 (Ref. 7). A central task has been developing a method for estimating true lateral displacements from the gravity-contaminated measurements. The method of analysis is exemplified by a set of data from Helland-Hansen (which had the best current measurements).

For a broader description of the VIV part of the Norwegian Deepwater Program, see Ref. 8.

The measurements

The instrument system to measure riser motion on Helland-Hansen consisted of six instrument containers attached to the riser in positions shown on **Fig. 1**. Each instrument unit con-

tained motion sensors, data acquisition hardware and batteries. The units were completely autonomous. The main sensors were accelerometers for measurement of horizontal acceleration in two orthogonal axes, *X* and *Y,* as shown in **Fig. 2**. In three of the instrument containers the accelerometers were supplemented with sensors for measuring angular velocity about the *X* and *Y*-axes. A seventh unit was installed in the drilling vessel. This unit was not used in the analysis.

The duration of the measuring period was about twelve weeks. All measuring units were in operation for about a month. Then intrument unit 1 failed, followed by unit 5 a few days later.

The instrument system and the collected data are described in detail in Ref. 6.

Current was measured by a number of acoustic doppler current profilers (ADCP) mounted in a vertical mooring in the neighbourhood of the drilling vessel. In addition to the ADCPs a rotor-type current meter measured current near the seafloor. The raw data consisted of readings every ten minutes, representing the average values of the ten-minute interval. The current data used in the analysis had been obtained by smoothing and interpolation (to fill "holes" in the data) in time and space and gave the speed and direction of the current at a number of depths. For the top 100 metres of the water column reliable current data could not be given due to disturbance from the drilling vessel's thrusters. After about eight weeks of operation the bottom meter failed.

Estimation of Riser Lateral Displacements

Accelerometer Signals. An accelerometer can measure true acceleration along its sensitive axis as long as the orientation of this axis is kept constant in space. For the accelerometers on the riser this will not be the case as the motion of the riser at any point will be a combination of sideways motion and rotation. That is, the centre line of the riser will deviate from the vertical causing the orientation of the accelerometer to deviate from the horizontal, thus exposing the sensing axis to gravity force. Assuming a small angle of rotation, it can be decomposed vectorally in rotations φ and θ about the horizontal axes *X* and *Y*, respectively. Letting $\ddot{x}$ and $\ddot{y}$ denote the components of true horizontal acceleration, the signals from the *X* and *Y* accelerometers will be

$$\begin{aligned} a_x &= \ddot{x} - g\,\theta \\ a_y &= \ddot{y} + g\,\varphi \end{aligned} \qquad \text{.....(1)}$$

where *g* is the gravitational acceleration (It is assumed that the *Z*-axis points upwards). Before the accelerometer signals can be integrated twice to give the lateral displacements the "disturbance" by gravity must be removed. Note that it is not possible to do this by conventional filtering, since the linear and angular motions will occur at the same frequencies.

If the riser moves at an *eigenmode* the translatory and rotary motions are linked together in a unique manner, i.e. knowing one means knowing the other. This can be extended to the case where the riser motion can be decomposed in a number *N* of eigenmodes. In this case (subject to certain restrictions) knowing the displacements at *N* points on the riser is equivalent to knowing the rotations at *N* points too. The principle of modal decomposition can be exploited further as described below.

Modal Approach. The modal decomposition is based on the assumption that any time-dependent shape of the riser can be expressed as a sum of eigenfunctions. For displacements in the *X* direction we get

$$x(z,t) = \sum_{n=0}^{\infty} q_n(t) d_n(z) \qquad \text{..... (2)}$$

where *z* denotes the vertical position on the riser (chosen positive upwards, zero at lower end) and $d_n(z)$ is the *n*-th eigenfunction. The variable $q_n(t)$ is the instantaneous magnitude (weight factor, modal participation factor, generalized coordinate) of the *n*-th mode. For displacements along the direction of *Y* there is a similar expression.

The inclination of the riser, i.e. the angular deviation from the vertical line, is obtained by differentiating (2) with respect to *z*. This gives

$$\theta(z,t) = \sum_{n=0}^{\infty} q_n(t) r_n(z) \qquad \text{..... (3)}$$

where

$$r_n(z) = \frac{d}{dz} d_n(z) \qquad \text{..... (4)}$$

is the eigenfunction of rotation which corresponds to $d_n(z)$.

For displacements along *X* the method for estimating true riser displacements is described in the following:

Let $z_1, z_2, z_3, z_4, z_5, z_6$ denote the positions of the instrument units on the riser. Inserting these coordinates in (2) and (3) gives the displacement and angle at the instrument positions. We want to express this in matrix notation and define the matrices

$$\begin{aligned} \boldsymbol{x} &= \left[x(z_1), x(z_2), x(z_3), x(z_4), x(z_5), x(z_6)\right]^T \\ &= \left[x_1, x_2, x_3, x_4, x_5, x_6\right]^T \\ \boldsymbol{q} &= \left[q_0, q_1, q_2, \ldots, q_N\right]^T \\ \bar{\boldsymbol{d}}_{\boldsymbol{n}} &= \left[d_n(z_1), d_n(z_2), d_n(z_3), d_n(z_4), d_n(z_5), d_n(z_6)\right]^T, \\ & \qquad\qquad n = 0,1,\ldots,N \\ \boldsymbol{D} &= \left[\bar{\boldsymbol{d}}_0, \bar{\boldsymbol{d}}_1, \bar{\boldsymbol{d}}_2, \ldots, \bar{\boldsymbol{d}}_N\right] \end{aligned} \qquad (5)$$

where it has been assumed that modes above the *N*-th mode do not contribute to the response. The mapping from modal weights to displacements at the given coordinates now becomes

$$\boldsymbol{x} = \boldsymbol{D}\boldsymbol{q} \qquad \text{..... (6)}$$

Likewise, the mapping from modes to angles can be written

$$\boldsymbol{\theta} = \boldsymbol{R}\boldsymbol{q} \qquad \text{..... (7)}$$

where $\boldsymbol{\theta}$ and $\boldsymbol{R}$ are defined in exact analogy with $\boldsymbol{x}$ and $\boldsymbol{D}$. Defining the vector of accelerometer signals

$$\boldsymbol{a} = \left[a_1, a_2, a_3, a_4, a_5, a_6\right]^T \quad \text{..... (8)}$$

the model for these measurements become (cf. Eq. 1):

$$\boldsymbol{a} = \ddot{\boldsymbol{x}} - g\boldsymbol{\theta} + \boldsymbol{\xi}_a = \boldsymbol{D}\ddot{\boldsymbol{q}} - g\boldsymbol{R}\boldsymbol{q} + \boldsymbol{\xi}_a \quad \text{..... (9)}$$

Here, ξ_a is a vector of measurement noise, which is necessary to make the picture complete. Further, considering the measurements of rate of rotation: Let ρ_1, ρ_2 and ρ_3 be the signals from the rotation rate sensors in instrument units 3, 4 and 6. We get the relation

$$\rho = \begin{bmatrix}\rho_1\\ \rho_2\\ \rho_3\end{bmatrix} = \begin{bmatrix}\dot{\theta}_3 + \xi_{\rho 1}\\ \dot{\theta}_4 + \xi_{\rho 2}\\ \dot{\theta}_6 + \xi_{\rho 3}\end{bmatrix} = \boldsymbol{S}\dot{\theta} + \boldsymbol{\xi}_\rho = \boldsymbol{S}\boldsymbol{R}\dot{\boldsymbol{q}} + \boldsymbol{\xi}_\rho \quad \text{..... (10)}$$

where $\boldsymbol{\xi}_\rho = \left[\xi_{\rho 1}, \xi_{\rho 2}, \xi_{\rho 3}\right]^T$ is measurement noise. $\boldsymbol{S}$ acts as a sifting matrix that sifts out the rotation rates that are measured, i.e.

$$\boldsymbol{S} = \begin{bmatrix}0\,0\,1\,0\,0\,0\\ 0\,0\,0\,1\,0\,0\\ 0\,0\,0\,0\,0\,1\end{bmatrix} \quad \text{..... (11)}$$

It is convenient to do the calculations in the frequency domain. Applying Fourier transformation to (9) and (10) gives

$$\begin{aligned}&\boldsymbol{a} = (-\omega^2\,\boldsymbol{D} - g\,\boldsymbol{R})\boldsymbol{q} + \boldsymbol{\xi}_a\\ &\boldsymbol{\rho} = -j\omega\boldsymbol{S}\boldsymbol{R}\boldsymbol{q} + \boldsymbol{\xi}_\rho, \qquad j = \sqrt{-1}\end{aligned} \quad \text{..... (12)}$$

where it is to be understood that the variables now are functions of frequency. Defining the combined vectors $\boldsymbol{m} = \left[\boldsymbol{a}^T, \boldsymbol{\rho}^T\right]^T$ and $\boldsymbol{\xi} = \left[\boldsymbol{\xi}_a^T, \boldsymbol{\xi}_\rho^T\right]^T$, Eq. (12) can be written as

$$\boldsymbol{m}(\omega) = \boldsymbol{G}(\omega)\,\boldsymbol{q}(\omega) + \boldsymbol{\xi} \quad \text{..... (13)}$$

where the matrix $\boldsymbol{G(\omega)}$, defined as

$$\boldsymbol{G}(\omega) = \begin{bmatrix}-\omega^2\,\boldsymbol{D} - g\,\boldsymbol{R}\\ -j\omega\,\boldsymbol{S}\boldsymbol{R}\end{bmatrix} \quad \text{..... (14)}$$

is the matrix transfer function from the vector of modal weights $\boldsymbol{q}$ to the measurement vector $\boldsymbol{m}$.

We want to determine the modal vector $\boldsymbol{q}$ from the measurement $\boldsymbol{m}$. To be able to do this, $\boldsymbol{q}$ must contain at most nine components, since there are nine measurements in $\boldsymbol{m}$ (six accelerations and three angular velocities). However, trying to estimate as many as nine modal variables will lead to noise-sensitive results. When fewer than nine modes are estimated (13) has to be solved in the least-squares sense, i.e. by minimising the quadratic scalar expression

$$J(\boldsymbol{q}) = \left[\boldsymbol{m}(\omega) - \boldsymbol{G}(\omega)\,\boldsymbol{q}(\omega)\right]^* \boldsymbol{W}\left[\boldsymbol{m}(\omega) - \boldsymbol{G}(\omega)\,\boldsymbol{q}(\omega)\right] \quad \text{... (15)}$$

with respect to $\boldsymbol{q}$. The asterisk denotes the combined operation of complex conjugation and matrix transposition. $\boldsymbol{W}$ is a diagonal weighting matrix, which is necessary when measurements of different type and magnitude are compared. Theoretically, the elements of $\boldsymbol{W}$ should be chosen as the standard deviations of the elements of $\boldsymbol{\xi}$, the measurement errors. As this information was difficult to assess, the following weight matrix was used instead:

$$\boldsymbol{W} = \mathrm{diag}(\sigma_a^{-2}, \sigma_a^{-2}, \sigma_a^{-2}, \sigma_a^{-2}, \sigma_a^{-2}, \sigma_a^{-2}, \sigma_\rho^{-2}, \sigma_\rho^{-2}, \sigma_\rho^{-2}) \quad (16)$$

Here σ_a is the largest standard deviation found amongst the members of $\boldsymbol{a}$, and σ_ρ is the largest standard deviation of angular velocity $\boldsymbol{\rho}$. The least squares solution for the modal weights is

$$\hat{\boldsymbol{q}}(\omega) = \left[\boldsymbol{G}(\omega)^*\boldsymbol{W}\,\boldsymbol{G}(\omega)\right]^{-1}\boldsymbol{W}\,\boldsymbol{G}(\omega)^*\boldsymbol{m}(\omega) \quad \text{..... (17)}$$

Finally, using (6) we get the estimate for the horizontal displacements, i.e.

$$\hat{\boldsymbol{x}}(\omega) = \boldsymbol{D}\hat{\boldsymbol{q}}(\omega) \quad \text{..... (18)}$$

Inverse Fourier transformation takes the displacements, as well any other result, to the time domain.

The estimation for the Y dimension is analogous. The only difference in the equations is that the sign of the matrix $\boldsymbol{R}$ must be changed.

Modeshapes. A number of *modeshapes* (eigenfunctions) for the riser at Helland-Hansen were computed using the finite element program RIFLEX (Ref. 10). The riser was modelled as correct as possible. The riser was pinned in two axes at both ends to prevent bending here. The tension at the upper end was assumed to be constant by means of a constant-tension device. The main riser data are shown in **Table 1**. The riser model was divided in elements of different length in such a way that the instrument containers were located in nodes between elements.

In the calculation zero damping was assumed. In addition to the calculated modeshapes, a straight-line shape was defined corresponding to a zeroth mode. The purpose of this mode was to be able to model the irregular slowly varying motion of the riser's upper end, which followed the movements of the dynamically positioned drilling vessel. **Fig. 3** shows the modeshapes corresponding to the six first modes including mode zero. The locations of the instrument containers are inicated by circles. It is seen that the modeshapes are almost sinusoidal in apperance, but not quite. The reason for this is the linearly increasing tension form bottom to top.

The modeshapes were calculated for a top tension of 4000 kN. This tension was the drilling company's best guess since the top tension was not recorded during drilling. Later, it became apparent that the real tension was most likely lower, per-

haps 3000 kN. An investigation shows that the calculated mode*shapes* are not very sensitive to the top tension. Besides, there are other incertaintes, such as the distribution of added mass and damping along riser, which may vary from case to case dependent on the current profile and the character of the VIV.

Mode selection and filtering. To use the least squares estimation technique described above, the modes one expects to find must be pre-selected. This could be done on basis of infromation given in the report from the instrumentation and data-acquisitioning report Ref. 6. For example, plots of the type shown in **Fig. 5** proved to be convenient. A study of this material showed that modes up to the fifth occured - the fifth only on rare occasions. While it was considered possible to estimate six modes simultaneously (the number of instrumented locations being six), this number was reduced to five to gain some extra robustness. Most of the time the analysis was done with modes {0,1,2,3,4}. For occasions when the fifth mode was present in the response and had to be included in the analysis one of the others was omitted, most often the 0^{th} mode. After instrument units 1 and 5 had failed, the number of modes to estimate was reduced to four.

To prevent the estimates of modal weights to be disturbed by signal components outside the frequency range that was relevant for the selected modes, the measurements were band-pass-filtered before use (Filtering the results would be equivalent). The cut-off frequencies of the bandpass filter varied with the chosen modes, but typically, the pass-band range was set to 0.01 - 0.16 Hz. The upper cut-off frequency could have been set to a lower value, preventing the wave-induced motion components to slip through. However, this was never a problem, as the least-squares estimation method performed well in every instance and had never any difficulty in producing results that seemed trustworthy.

Verification of the method. The method for estimating riser modes and displacement was tested on simulated measurements of acceleration and rate of rotation. The simulation was done with RIFLEX. The simulated measurements included the contribution from the *g* component. The estimation method was able to recreate the true motion perfectly.

Current analysis

The purpose of the current analysis was to find the best 2-dimensional representation of the measured profile as a preparation for the model verification. In addition a number of characterising parameters were calculated as described in the following.

Main Direction. Analysing the measured riser motion in a coordinate system that is rotated such that one axis points in the main current direction may be useful because most prediction tools are based on a 2-D current profile, and the riser may behave as if the profile be 2-D at least in some cases. Thus, by transforming the current and the measured riser data into the new coordinate system determined from the current profile, it may be easier to see the essential behaviour of the riser.

The riser motion is measured in a coordinate system *XY* which is defined by the orientation of the instrument cylinders, see **Fig. 2**. A new coordinate system X_CY_C is found by a counterclockwise rotation about the vertical axis. The axis X_C is defined as the principal or main current direction and axis Y_C is normal to the principal direction. The idea is to rotate the new coordinate system until the average velocity component along axis Y_C becomes as small as possible in the least squares sense. This is done as follows.

The current profile is given for a number of depths, i = 1, 2,..., n. Let (x_i, y_i), i = 1, 2,..., n, denote the current profile as given in riser coordinates, i.e. with respect to *XY*. Let ($x_{C,i}(\alpha)$ $y_{C,i}(\alpha)$) be the representation of the profile in axes X_CY_C which are rotated an angle α relative to *XY*. We want to determine α such that

$$\sum_{i=1}^{n} y_{C,i}^2(\alpha) \qquad \text{..... (19)}$$

becomes minimum. The minimum is obtained for

$$\alpha = \tfrac{1}{2}\tan^{-1}\left(\frac{\sum_{i=1}^{n} 2x_i y_i}{\sum_{i=1}^{n}(x_i^2 - y_i^2)}\right), \text{ if } \sum_{i=1}^{n}(x_i^2 - y_i^2) > 0 \qquad (20)$$

or

$$\alpha = \tfrac{1}{2}\tan^{-1}\left(\frac{\sum_{i=1}^{n} 2x_i y_i}{\sum_{i=1}^{n}(x_i^2 - y_i^2)}\right) + \frac{\pi}{2}, \text{ if } \sum_{i=1}^{n}(x_i^2 - y_i^2) < 0 \qquad (21)$$

Some characteristic parameters are calculated from the transformed current profile.

Three-Dimensionality. One measure describing the amount of the horizontal current that is not in the main direction is given by a spread parameter, *D,* defined as follows:

$$D = \frac{rms(y_C)}{rms(x_C)} = \sqrt{\frac{\sum_{i=1}^{n} y_{C,i}^2}{\sum_{i=1}^{n} x_{C,i}^2}} \qquad \text{.....(22)}$$

Note that the velocities are squared in the equation, which means that the sign of the velocities does not influence the spread parameter. The basis for this choice is that the shedding process is assumed to be insensitive to the sign of the velocity. For a pure 2-D current profile *D* becomes zero. For a case with rms(y_C) equal to rms(x_C) *D* becomes unity.

Shear. Vandiver (Ref. 7) has defined the shear of a current profile as the ratio between the velocity variation ΔU and the

average velocity U_{mean}, i.e. $S_V = \Delta U / U_{mean}$. In many of the observed current profiles, the variation of current velocity varied a lot with a rather random pattern and a more general shear parameter is therefore defined:

$$S = \frac{\sigma_{x_C}}{\bar{x}_C} = \frac{\sqrt{\frac{1}{n}\sum_{i=1}^{n}(|x_{C,i}| - \bar{x}_C)^2}}{\frac{1}{n}\sum_{i=1}^{n}|x_{C,i}|} \quad \text{.....(23)}$$

where the horizontal bar denotes mean value. S expresses the non-dimensional amount of variation of the absolute current velocity about the mean absolute velocity. The sign of the velocity is neglected for the same reasons mentioned before. For a linearly varying current profile the relationship between S_V and S is

$$S_V = 2\sqrt{3}\,S \cong 3.5\,S \quad \text{.....(24)}$$

Selection of cases for analysis

The Helland Hansen data consists of 916 sets of records of riser measurement, each of 34 minutes length. To avoid putting uninteresting cases through the mill of analysis a criterion for selection was needed. Of special interest are cases showing lock-in.

A statistical analysis of the acceleration data had been performed in Ref.6. A study of how to pick out interesting cases from this statistical data was performed. This study showed that the value of the *kurtosis* gives an indication of when lock-in happens (see Ref. 9).

Kurtosis is defined as m_4/m_2^2, where m_4 and m_2 are the 4th and 2nd moments of the signal's distribution, respectively. For a Gaussian process, as is typical of multi-frequency random vibrations, the kurtosis value is 3.0. For a sinusoidal process, as is typical for a single mode lock-in event, the kurtosis value is equal to 1.5. Hence, if the kurtosis of a representative measurement is plotted as function of time interesting records may be picked out by looking for low kurtosis values. **Fig. 4** shows the kurtosis and the standard deviation based on the accelerometer signal from measurement unit number 2.

Also the variation in response frequencies and which modes participate in the motion are of interest. This information was obtained from colour-coded spectral plots found in Ref. 6. **Fig. 5** is one example (colour not shown in the print). The white specks in the figure indicate the spectral peaks. An oscillating behaviour of the peak frequencies of modes 2 and 3 due to the tidal cycle is easily seen.

It was of interest not only to study single events, but also how phenomena develop with time, e.g. investigate mode transitions from one record to the next and the circumstances under which they occur, notably changes in the current profile. Therefore, instead of choosing a number of isolated single events, a certain 'neighbourhood' around each case was required. Ten blocks of contiguous records where picked out. In total, the blocks comprise 357 sets of records.

Results

An example. The results for each analysed case were presented on four different sheets with figures. **Figs. 6-9** show an example of these sheets, representing 2nd-mode lock-in case.

Fig. 6 presents the current situation for the actual case. The figure is split into four sub-plots. The upper left sub-plot shows a polar plot of the current flow in a horizontal projection. The principal direction of the current is shown as a radial line. The upper right plot presents the current profile projected onto the principal plane, i.e. vertical plane extending in the principal direction (along axis X_C). The lower left plot is the normal projection of the current profile (along Y_C), i.e. the spreading profile. The lower right sub-plot shows the total speed profile.

The figure shows an example of a nearly uniform and 2-D current. The maximum velocity and mean velocity in the principal plane are 0.23 and 0.19 m/s, respectively. The shear coeffient (cf. Eq. 23) is 0.15. The spreading coefficient (according to Eq. 22) is as low as 0.1. The spreading profile indicates that the current is rotated a little as depth increases.

Fig. 8 shows the estimated displacements of the riser at the instrumented locations. The displacements are calculated using (2) with the sum taken over the participating modes. The left part of the figure presents a section of the estimated displacements. The right part of the figure shows the corresponding amplitude spectra. The relationship between the amplitude spectrum, $a(f)$ and the more commonly used power density spectrum, $S(f)$, is

$$a(f) = \sqrt{2S(f)\Delta f} \quad \text{..... (25)}$$

where Δf is the frequency spacing. The amplitude spectrum is selected to present the frequency information because it shows small spectral values better than the power spectrum does. Also, it gives the benefit that the magnitude of $a(f)$ is directly comparable to the displacements in the corresponding time trace on the left. The upper part of the figure shows the in-line displacement (in the X_C direction) and the lower part shows the transverse displacements (in the Y_C direction).

Fig. 9 is identical to Fig. 8, except that it shows the modal weights as functions of time and not displacements.

Fig. 7 shows some statistical results together with X_CY_C-plots of displacement. The two upper left sub-plots show the rms profiles of the riser displacement, i.e. how the rms value of displacement varies along the length of the riser. The locations of the instrument units are indicated by circles. Note that for a single-frequency response the amplitude at any point on the riser is 1.4 times the rms value. The rms values of the modal weight factors are presented in the two bar plots in the lower left part of the figure. The six small plots to the right in the figure show the horizontal trace of the riser motion at the instrumented locations. The principal current direction is along the positive X_C axis in the figures and consequently the transverse motion is in the Y_C direction. Note that mode number 0 has not been included in the rms profiles and the X_CY_C plots

since it does not represent a proper mode.

For the calibration of the VIV models, the current profiles (Fig. 6) and the riser motion rms profiles (Fig. 7) are intended as the main information.

Discussion. The case shown in Figs. 7, 8 and 9 is a clear example of a 2nd-mode lock-in. From Fig. 8 it is seen that the dominating motion component has a frequency between 0.05 and 0.06 Hz (the exact value was found to be 0.0561 Hz). Further, some low frequency components are shown on the spectra, seemingly increasing towards the top. This indicates that the source of these components is the irregular slowly varying motion of the drilling platform. The effect of the band-pass filtering is clearly seen as the abrupt cut-off at 0.01 Hz (The upper filtering frequency of 0.16 Hz is outside the plotted range).

The plots of time traces and spectra for the estimated modal weights (Fig. 9) show that the motion is indeed 2nd mode. Hence, the method of estimation seems to be successful.

It is further shown that mode zero has been allotted most of the low frequency motion components that follow from the vessel's motion. This is exactly as intended. While good, the result is not perfect. There is a noticeable amount of 0.0561 Hz oscillation on the estimates of other modes than the second. It is possible that a recalculation of the modeshapes with a lower and probably more correct top tension would have changed this and produced a "cleaner" 2nd-mode response. This was not tried, however. On the other hand, on physical grounds one cannot expect that a motion consisting of the 2nd natural frequency will take place at the 2nd modeshape only. The geometry of the VIV will also depend on how the excitation and damping forces are distributed along the riser. In general one will expect to see other modeshapes in action as well.

The rms profiles and bar plots in Fig. 7 confirm the 2nd-mode character of the motion. However, it seems that the main current direction as determined from the current (Eq. 20 and 21) and used to define the direction of axis X_C does not completely separate the in-line and cross-flow directions. This is also confirmed by the six small figures to the right in Fig. 7. Ideally the long axes of the motion ovals should appear vertical on the plots. The reason why this does not happen may be some inaccuracy in measured current direction. It is interesting to note that the motion ovals seem to rotate some from bottom to top. This agrees well with the rotation of the current as it appears from Fig. 6.

Comparison between response parameters and current. To demonstrate some characteristic relationships from the analysed lot of records a 3-day span of time is chosen. This gives a suitable time scale on the figures. It is interesting to see how the modes vary with time on this scale. Quantifying the magnitude of a mode can be done in different ways. A natural choice is the rms value. The term "mode" itself can be ambiguous. One way to look at "mode" is to tie it to the modeshape. In this way the magnitude of the mode can be calculated as the rms value of the modal weight (= participation factor), i.e. the function $q_n(t)$ as defined by (2). Put differently, the definition gives the magnitude of the time variation of a certain *modeshape*, regardless of frequency. The bar plots in Fig. 7 show mode magnitude according to this definition.

The alternative definition of "mode" is to tie it to natural frequency. In this way a measure of the magnitude of a mode can be calculated as the square root of the power of all oscillation components taking place at the mode's natural frequency (or in a narrow band around it), regardless of modeshape. In the case of non-lock-in riser motion consisting of non-standing wave patterns, the latter definition may be the most informative, and was chosen for the representation in **Fig. 10**. This figure shows the magnitudes of participation of modes 1–5. The mode participation includes both the in-line and transverse components of motion. Also kurtosis is shown, based on the signal from one of the accelerometers in instrument unit 2 (Fig. 1). This is the same kurtosis that was used in the process of picking cases for analysis. The figure demonstrates that mode 2 and mode 3 are in anti-phase. Also, mode 3 is in anti-phase with kurtosis. This indicates that when mode 3 dominates there is lock-in (i.e. low kurtosis values) while mode 2 is dominant in the non-lock-in cases (This of course, applies to the example shown and is not a general statement about the character of VIV). Further, the figure shows that about midday on the third day mode 4 takes over. From then it seems to be alternating with mode 3. Modes 1 and 5 are so small that they are not visible on the figure.

With regard to kurtosis as a marker for lock-in, the examples in Fig. 10 seem to support it. However, the kurtosis criterion it is not infallable as there are also occurences with single frequency motion and relatively high kurtosis. The reason for this may be that the envelope of the motion varies somewhat within the 34 minutes period of each record. One example is the case shown in Fig. 8-9. The motion is clearly 2nd mode, but the kurtosis was found to be 2.36.

Fig. 11 supplements the information in Fig 10. This figure shows the variation of the dominating frequency of vibration together with the maximum speed of the current. It is striking how the frequency depends on the current speed. It is clearly seen that three separate levels of frequency exist, corresponding to modes 2, 3 and 4. Some variation within each level can also be seen. This is typical of VIV. Even when the structural properties of the riser stay constant (e.g. the top tension), the current-dependent hydrodynamic nature of VIV is capable of shifting the natural frequency up or down such that it may coincide with the vortex-shedding frequency. The result in Fig. 11 indicates that the measurements of riser motion and current are of good quality.

Table 2 shows how frequency can vary. Based on the processed cases, the table gives the range of each natural frequency. It is noted that there is no overlap beteeen the frequency intervals.

The frequency spread in Table 2 may also include effects that are not caused by the current, as the following example

shows: A sudden change in the eigenfrequencies was detected between 8 and 10 p.m. at May 4. The drilling log showed that before the change in the eigenfrequency, the drill collar was inside the riser and afterwards it was in the drilling hole. This made a significant difference to the weight of the riser before and after the incident, and hence, a change in the eigenfrequencies occurred. This incident could clearly be seen on spectrum plots similar to the one shown in Fig. 5. The example shows that any interpretation as to the causes of phenomena related with VIV should wait till the drilling log has been studied.

While Fig. 11 shows very good correlation between current speed and frequency of riser oscillation it was not difficult to find other examples where the correspondence was not so good. The reasons for this may be variations in the degree of complexity of the current profile, i.e. variations in shear and 3-dimensionality. Also, a reason may be that the quality of the current data varied.

To further investigate the dependence of frequency on current a number of single-frequency VIV cases were selected. Average speed and maximum speed were chosen as the characterising parameters of the current. **Fig. 12** shows the eigenfrequencies plotted against mean speed. In **Fig. 13** the eigenfrequencies are related to maximum speed. In both figures the theoretical relation between frequency and current speed is shown as a straight line, assuming a value of 0.23 for the Strouhal number.

The figures clearly show that the maximum current speed gives the better agreement with the theoretical line. Still the spread is large. This is not unexpected, since it is only reasonable that more parameters are needed to characterise the current, e.g. the coefficients of spreading (21) and shear (22).

Conclusion

For verification of VIV-prediction tools full-scale riser motion data and depth profiles of current are required. When accelerometers are used for measurement of riser motion, the signals will in general be contaminated by the time-varying influence of the gravitational acceleration as a result of the riser's angular motion. A method for correcting this disturbance and estimating true riser displacements is described. The method uses modal decomposition in combination with a least squares estimation technique. In addition to measured acceleration the method can include signals from rotation rate sensors. The estimation method has been applied to a large amount of full-scale measurements in order to prepare data for verification of VIV-prediction software. The method performs well. From the current measurements the current's main direction, amount of shear and three-dimensionality were computed. The main input to the verification are corresponding current profiles and riser rms profiles. To sort out lock-in cases for analysis the concept of kurtosis has proven useful. This is because low kurtosis values usually are connected with lock-in events. A comparison between VIV frequency and maximum current speed, shows clear correlation. Still there is considerable scatter, which must be owing to other properties of the current profile.

Nomenclature

a = acceleration signals from accelerometers, L/t^2 ,m/s^2.
$a(f)$= amplitude spectrum.
d_n = eigenfunction of diaplacement.
D = spread parameter.
$\boldsymbol{D}$ = matrix of the eigenfunctions of displacement at the position of the measurement units.
f = frequency, t^{-1}, s^{-1}.
F = frequency, t^{-1}, Hz.
Δf = frequency spacing, t^{-1}, Hz.
g = gravitational acceleration, L/t^2, m/s^2.
$\boldsymbol{G}$ = matrix transfer function from vector of modal weights to measurement vector.
j = unit of imaginary numbers.
m_2 = 2nd spectral moment.
m_4 = 4th spectral moment.
$\boldsymbol{m}$ = vector of measured accelerations and rotation rates.
N = number of modes.
q = modal weight = modal participation factor.
$\boldsymbol{q}$ = vector of modal weights.
r = eigenfunction of rotation.
$\boldsymbol{R}$ = matrix of the eigenfunctions of rotation at the position of the measurement units.
S = shear parameter.
$S(\omega)$= power density spectrum.
S_V = shear parameter as defined by Vandiver, Ref.2.
$\boldsymbol{S}$ = sifting matrix.
t = time, t, s.
U_{mean}= average current speed, L/t, m/s.
ΔU = velocity variation, L/t, m/s.
$\boldsymbol{W}$ = weighting matrix.
x = x-component of true horizontal displacement, L, m.
$\ddot{x}$ = x-component of true horizontal acceleration, L/t^2, m/s^2.
y = y-component of true horizontal displacement, L, m.
$\ddot{y}$ = y-component of true horizontal acceleration, L/t^2 , m/s^2.
X,Y = reference axes for riser motion measurements.
$x_i y_i$ = current profile in measurement coordinate system.
X_C, Y_C = reference axes for current. X_C is main direction.
$x_{C,i} y_{C,i}$ = current profile in current axes
z= vertical position on the riser, L, m.
α = angle between riser X-axis and main direction of current .
φ = rotation about the riser X-axis.
θ = rotation about the riser Y-axis.
ξ = measurement noise.
ξ_a = measurement noise on accelerations.
ξ_ρ = measurement noise on rotation rates.
ρ = signal from rotation rate sensors.
σ_a = the largest standard deviation of acceleration.
σ_ρ = the largest standard deviation of rate of rotation.
ω = frequency, rad/s.

Subscripts

a = acceleration.
C = current (in-line, transverse) axes.
n = eigenfunction number.
ρ = rotation rate
i = current measurement number (depth number).

Acknowledgments

The work described in this paper was carried out as a part of the Norwegian Deepwater Program (NDP). Partners in the NDP group were BP Amoco, Conoco, Exxon, Mobil, Norsk Hydro, Saga, Shell, and Statoil. The authors thank Corrocean Robit Technology AS for figure material from their instrumentation and data acquistion report (Ref. 6).

References

1. Gopalkrishnan, R.: "Vortex-Induced Forces on Oscillating Bluff Cylinders", Doctoral Thesis, Massachusetts Institute of Technology and Woods Hole Oceanographic Institution, February 1993
2. Vikestad, K.: "Multi-Frequency Response of a Cylinder Subjected to Vortex-Shedding and Support Motions", Doctoral Thesis, Norwegian University of Science and Technology, Trondheim, 1998
3. Lie, H. and Vandiver, J., K.: "VIV Model Test of a Bare and Staggered Buoyancy Riser in a Rotating Rig", Paper OTC 8700, Offshore Technology Conference, Houston, 1998.
4. Blevins, R., D.: "Flow-Induced Vibration", 2nd Ed., Van Nostrand Reinhold, New York, 1990
5. Vandiver, K.: "Research Challenges in the Vortex-Induced Prediction of Marine Risers", Paper OTC 8698, Offshore Technology Conference, Houston, 1998.
6. Pettersen, B., Saudland, A.: "NDP Risers and Moorings Project. Monitoring of VIV on Drilling Riser on Helland Hansen," Technical Report, TR066980, CorrOcean Robit Technology AS, Oslo, 1998.
7. Vandiver, J.K. and Li, I.: "Vortex Induced Vibrations of Cylinders SHEAR7 Program, Users Manual," Massachusetts Institute of Technology, Cambridge, Massachusetts, 1994.
8. Halse, K., H.: "Norwegian Deepwater Program: Improved Prediction of Vortex-induced Vibrations", Paper OTC 11996, Offshore Technology Conference, Houston, 2000
9. Vandiver, J.K., "Predicting Lock-in on Drilling Risers in Sheared Flows", Proc. Flow-Induced Vibrations 2000 Conference, Lucerne, June 2000.
10. RIFLEX Program Documentation. SINTEF, Trondheim, Norway, 1995.

SI Metric Conversion Factors

ft	× 3.048*	E-01 = m
ft^2	× 9.290 304*	E-02 = m^2
ft^3	× 2.831 685*	E-02 = m^3
lbf	× 4.448 222*	E+00 = N
lbs	× 4.535 924*	E-01 = kg

Table 1 – Riser data

Riser length (m)	682.75
Submerged length (m)	670.46
Length of part with buoyancy at lower end (m)	34
Length of part with buoyancy at upper end (m)	100
Total length with buoyancy (m)	503
Outer diameter, bare riser (m)	0.5334
Inner diameter, bare riser (m)	0.5017
Outer diameter of riser + buoyancy (m)	1.1303
Mass per length unit, bare incl. mud (kg/m)	720.53
Mud density (kg/m^3)	1420
Axial stiffness (N)	5.42E+09
Bending stiffness (N)	1.82E+08
Pretension in upper end (kN)	4000

Table 2 – Frequency ranges of modes 1-5 (Hz)

f_1	0.022 - 0.031
f_2	0.047 - 0.056
f_3	0.071 - 0.079
f_4	0.100 - 0.110
f_5	0.120 - 0.130

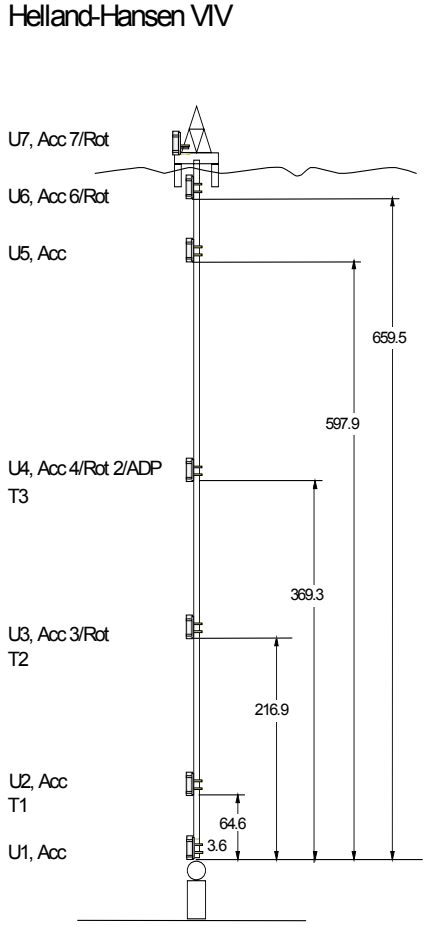

Fig. 1 - Instrument position on the Helland Hansen riser. U1, U2 and U5 contain accelerometers. U3, U4 and U6 are in addition supplemented with sensors for measuring angular velocity. U7 is installed in the drilling vessel (From Ref. 6).

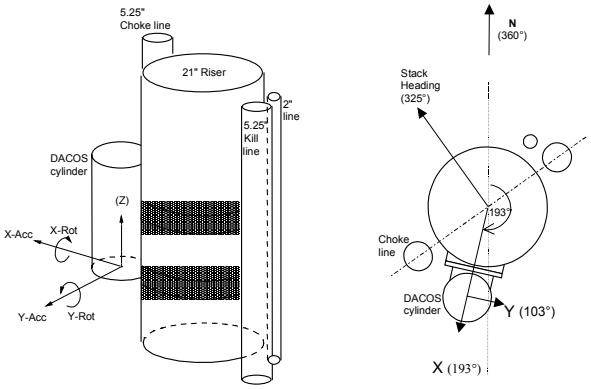

Fig. 2 - Orientation of instruments on the riser (From Ref. 6).

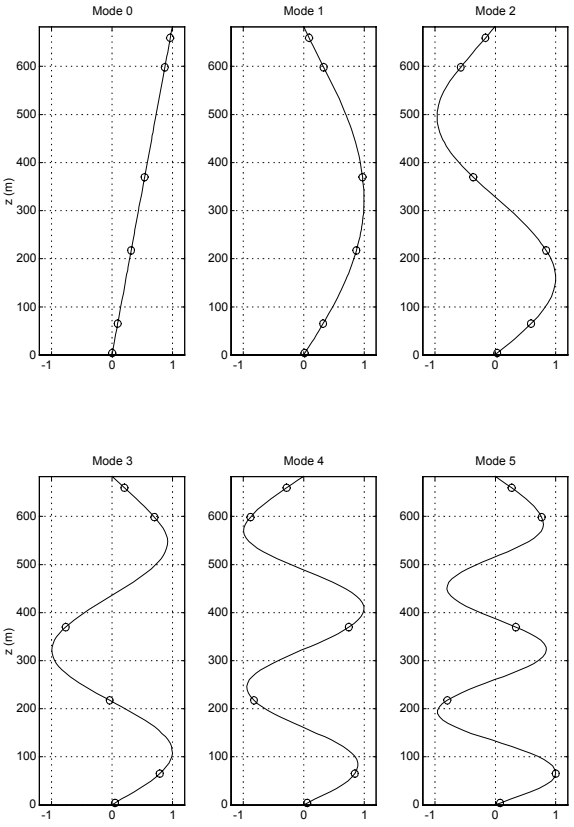

Fig. 3 - Modeshapes of riser displacement.

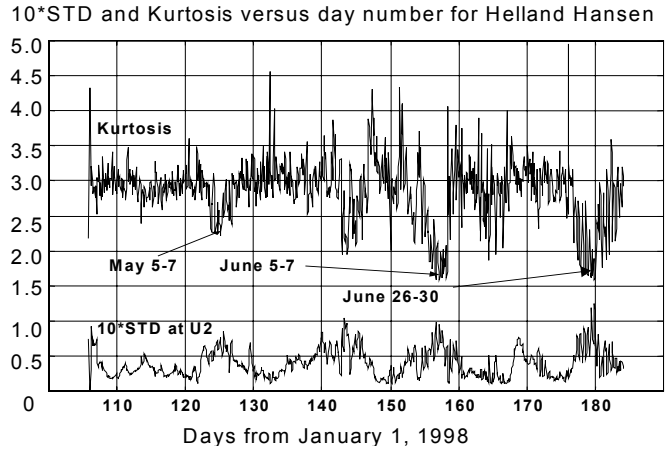

Fig. 4 - Standard deviation and kurtosis for measurement unit number 2 as function of day number.

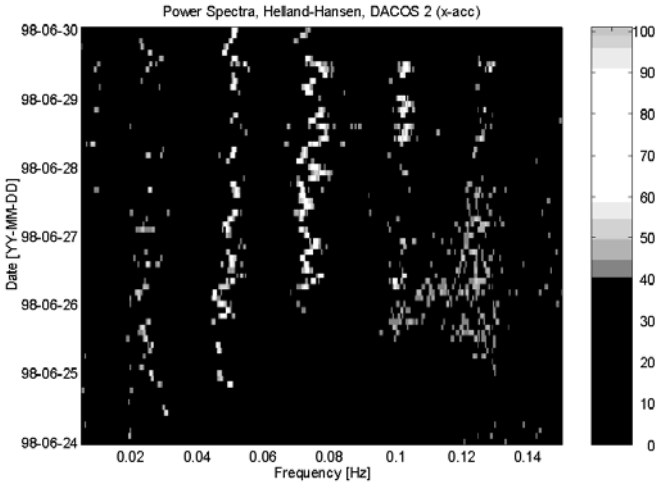

Fig. 5 - Power spectra for acceleration in X-direction for measurement unit number 2. (From Ref. 6).

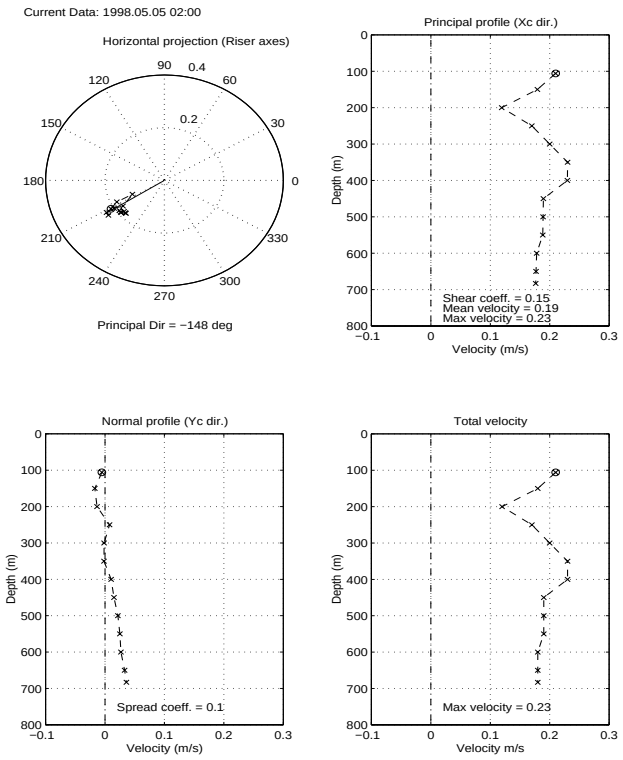

Fig. 6 - Current profile and data.

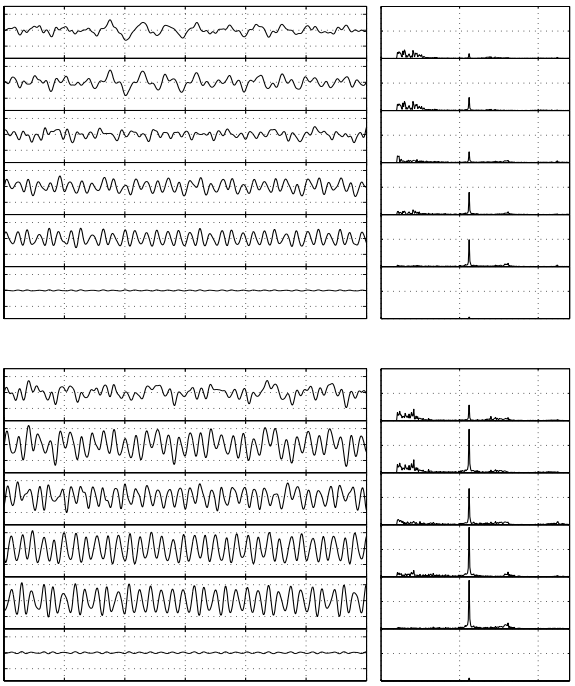

Fig. 8 - Estimated displacement and amplitude spectrum at instrument locations.

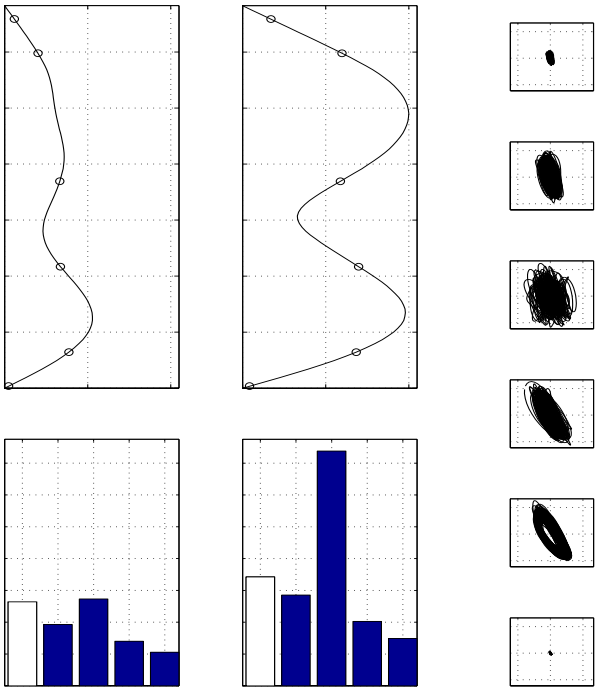

Fig. 7 - RMS-profile of riser displacement, modal weights and xy-plots of riser displacements at instrument locations.

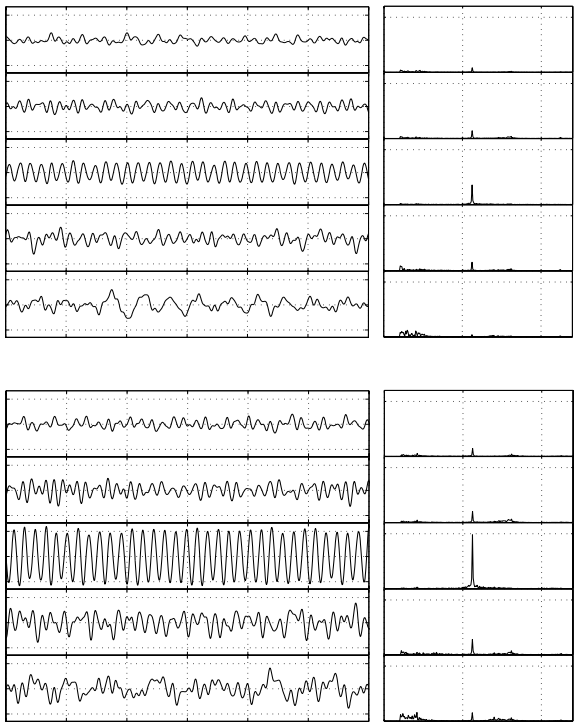

Fig. 9 - Time series and amplitude spectra of modal weights.

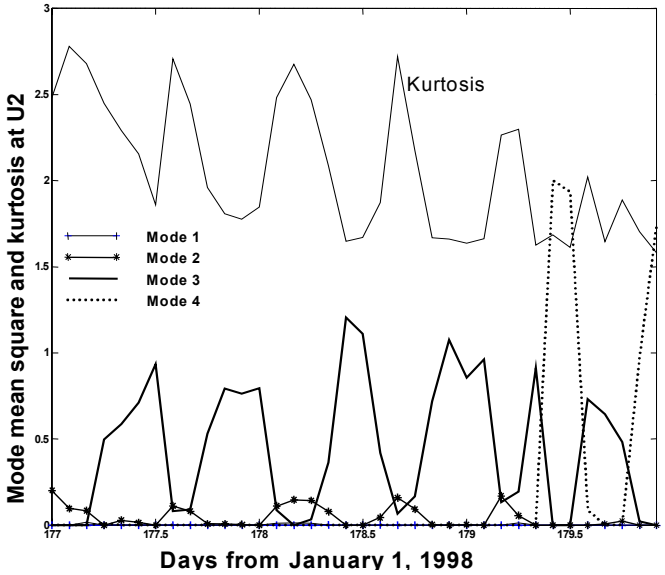

Fig. 10 - Mode participation and kurtosis

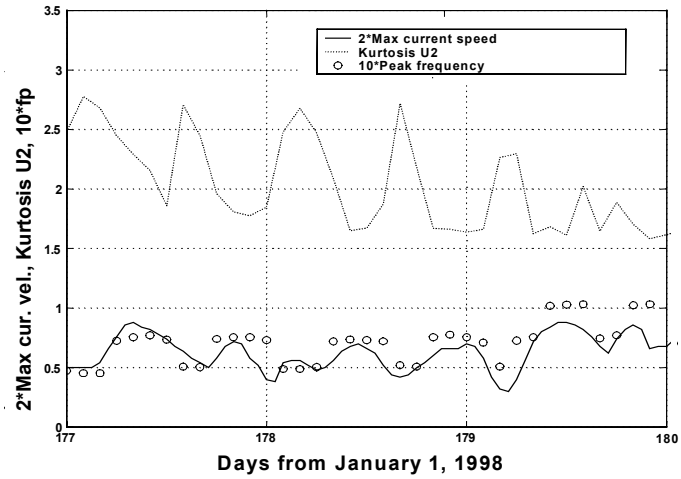

Fig. 11 - 2 times maximum current velocity, kurtosis and 10 times the peak frequency.

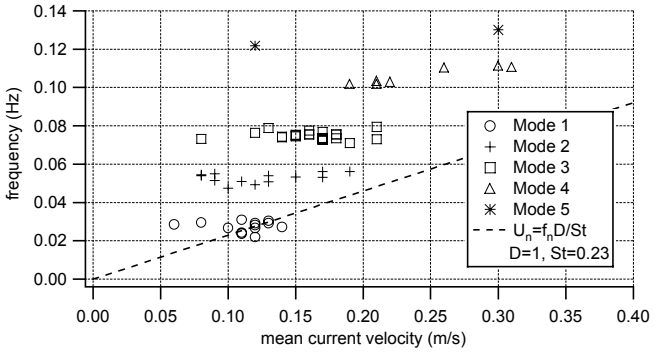

Fig. 12 - Frequency of dominating mode as function of mean current speed.

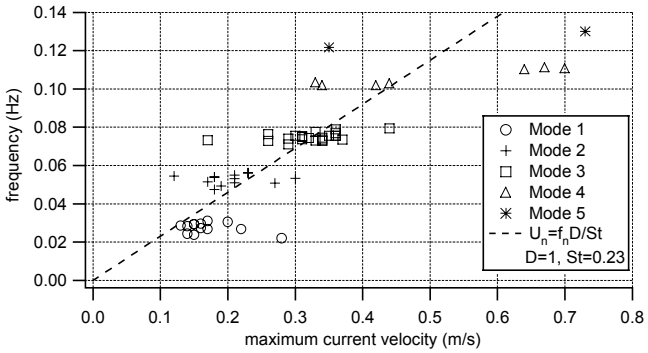

Fig. 13 - Frequency of dominating mode as function of maximum current speed.